Titre: Title:	Variable refrigerant flow heat pump model with estimated parameters and emulated controller based on manufacturer data
Auteurs: Authors:	Aziz Mbaye, & Massimo Cimmino
Date:	2022
Type:	Communication de conférence / Conference or Workshop Item
Référence: Citation:	Mbaye, A., & Cimmino, M. (2022, September). Variable refrigerant flow heat pump model with estimated parameters and emulated controller based on manufacturer data [Paper]. 5th Building Performance Analysis Conference and SimBuild (2022), Chicago, Illinois (18 pages). Published in Science and Technology for the Built Environment, 30(4). https://doi.org/10.1080/23744731.2023.2279469

Variable refrigerant flow heat pump model with estimated parameters and emulated controller based on manufacturer data

A new physics-based and modular variable refrigerant flow (VRF) heat pump model aimed towards multi-year simulations is presented. The model allows the simulation of any number of indoor units (IU), outdoor units (OU) and compressors. A parameter-estimation procedure and a control strategy both using available manufacturer data is proposed. The model is validated against data collected from a VRF system that services the first floor of the former ASHRAE Headquarters Building in Atlanta (USA), comprised of 22 indoor units, 2 outdoor units and 8 compressors. Results show that the model accurately predicts the total energy consumption over a 2-month cooling period, with a relative error, normalized mean bias error (NMBE), and coefficient of variation of the root mean square error (CVRMSE) of 1%, 1.6%, and 16.7%, respectively.

Keywords: variable refrigerant flow; heat pump; model calibration; controller emulation

1. Introduction

Variable Refrigerant Flow (VRF) heat pumps are advanced heat pump systems designed to provide heating and cooling in commercial and institutional buildings. Although conventional heat pump technology has been around for almost 70 years, VRF systems were not introduced until the late 1980s (Goetzler, 2007). Since then, their popularity has continued to increase. A typical VRF system consists of an outdoor unit (OU), several indoor units (IU) distributed throughout the building, and a piping network that facilitates the refrigerant flow between the outdoor and indoor units. When equipped with a heat recovery unit, VRF systems can simultaneously provide heating and cooling to different zones within the same building, and they can also recover and redistribute heat between zones for greater energy efficiency.

The design of a VRF system is heavily influenced by the building's unique architecture, which affects the system's size (i.e., number of indoor units), performance

(i.e., the energy consumption of the system), operation and the piping layout. Due to this complexity, engineers and HVAC professionals have identified some limitations of VRF systems, particularly because their design and operation rely on proprietary software from manufacturers (Petrus, 2021). This reliance ties the system to a particular manufacturer from the early design stages, which can be problematic. To support the continued development of VRF systems, it is essential to have non-proprietary and validated simulation tools that can facilitate their design and evaluate their performance.

VRF models range from detailed physics-based models to equation-fit models with varying levels of accuracy (Lin et al., 2015). Physics-based models represent the behavior of VRF systems using thermodynamic first principle equations and have shown to predict systems operation with good accuracy (Hong et al., 2016). These models are usually developed for the simulation of systems with limited number of indoor units (Wu et al., 2005) since they are computationally expensive. Some authors have proposed modular VRF models that are independent of the number of indoor and outdoor units (Zhu et al., 2013) and generalized for systems with arbitrary configurations and layouts (Sun et al., 2017). However, these models are validated using data collected on systems with a small number of indoor units. The largest validation studies found in the literature for such modular models consists of VRF systems with 1 outdoor unit and 4 indoor units (Hong et al., 2016; Sun et al., 2017). Hong et al. (2016) analyzed the VRF total energy consumption over a 17-day cooling period. The comparison results for an hourly time scale revealed a relative error of 2%, a normalized mean bias error (NMBE) of 2.8%, and a coefficient of variation of the root mean square error (CVRMSE) of 14.6%. Physics-based VRF models are also used to assess some operation characteristics such as the effect of the pressure drop and the refrigerant piping length on the system's performance (P. Yan et al., 2012). However,

these models require data, such as component model parameters that are unavailable, especially for commercial VRF systems since they are not readily provided in manufacturer literature.

Empirical equation-fit models are more popular for VRF systems simulation because they are based on performance curves using available manufacturer data. Moreover, they are a less computationally expensive approach. This very reason explains why prominent building energy simulation tools, including EnergyPlus (Raustad, 2013) and eQUEST, exclusively incorporate Empirical VRF models. Y. Li et al. (2009) introduced an equation-fit model tailored for water-cooled VRF air conditioning systems. This model builds upon a prior air-source VRF model developed by Zhou et al. (2007) and is also implemented within EnergyPlus. Compared to the physics-based models, equation fit models predict VRF total energy use with less accuracy. Comparison studies against field-test data show a daily energy use relative error within the range of 25% (Sharma & Raustad, 2013) or between 15% and 45% (Zhou et al., 2008).

Calibration is a method that can improve the accuracy of energy simulation models (Reddy, 2006). VRF equation fit models have been shown to benefit from calibration in several studies (Kim et al., 2018; Pachano et al., 2022; Yun & Song, 2017), particularly when the building envelope model is included. Calibration procedures for equation fit models include the determination of operating conditions (i.e., setpoint temperatures and air flow rates) (Yun & Song, 2017), the adjustment of performance curve coefficients (Pachano et al., 2022) and the modification of heating and cooling coefficient of performance (COP) (Kim et al., 2018). However, these methods require measured data from the specific building where the VRF system is installed, which limits their generalizability. Additionally, such calibration during the

HVAC system design stage may be challenging due to the need for onsite measurements. Cheung and Braun (2014) introduced a comprehensive gray-box, component-based model for Variable Refrigerant Flow (VRF) systems, encompassing models for the refrigerant pipeline, refrigerant accumulator, and electronic expansion valve (EEV). The calibration process of this model involves a two-tier process: parameter tuning at the component level and performance adjustment at the system level through parameter multipliers. This calibration method necessitates specific system data, such as compressor speed, suction pressure, subcooling values for units operating as condensers, refrigerant mass flowrate, and pipeline geometry (including diameter and length). Comparative analysis with data obtained from a dual unit VRF system operating in heating mode highlights enhanced predictive accuracy in power consumption achieved through the model.

Existing VRF models have demonstrated limitations when applied to systems with a substantial number of indoor units:

(1) VRF systems that are designed using equation-fit models typically require oversizing to compensate for their lower accuracy, which stands at around 25% (Sharma & Raustad, 2013). This oversizing can affect the cost effectiveness of these systems.

(2) While physics-based models generally provide superior predictive accuracy in comparison to equation-fit models, their limitation lay in their applicability to large commercial VRF systems due to both the high number of parameters and their limited availability.

(3) The inherent complexity of physics-based models tends to result in extended computational times, which, in turn, diminishes their suitability for multi-year simulations.

(4) Validation of existing models has, thus far, relied on data obtained from systems featuring a limited number of units. As a result, their ability to scale effectively to large systems remains unverified.

In response to these shortcomings, this paper introduces a novel VRF heat pump model designed specifically for simulating large systems with many indoor units. To ensure the availability of parameters, this new model relies on a simplified thermodynamic cycle and incorporates a parameter estimation procedure and control strategy that leverage manufacturer data. The simplified cycle also helps in reducing the number of model parameters and contributes to a decrease in computation time. The validation of the model is conducted in cooling mode, utilizing data from a system consisting of 22 indoor units. This data is monitored data from the HVAC systems at the former ASHRAE Headquarters Building in Atlanta (USA).

2. Model

2.1. Modeling approach

The studied VRF heat pump system includes multiple IUs, and an OU with several compressors operating in parallel as well as a heat exchanger. This system is illustrated in Figure 1. The new model aims to simulate the energy performance of such systems during multi-year operation.

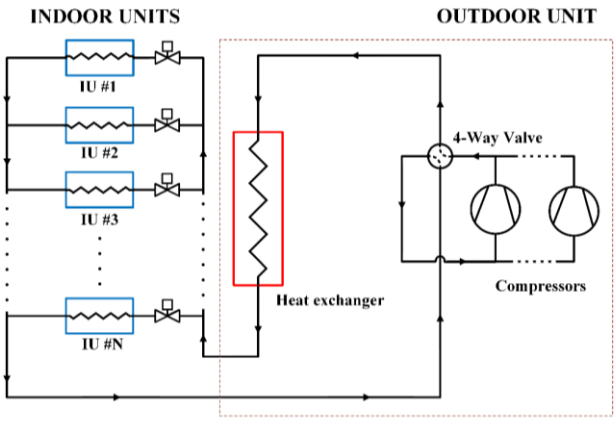

Figure 1. Schematic diagram of the studied VRF system.

Classified as a physics-based model, the proposed VRF model is based on a simplified vapor compression cycle as proposed by Jin and Spitler (2002). Figure 2 presents the pressure-enthalpy diagram of this simplified thermodynamic cycle that relies on the following assumptions:

- At the evaporator outlet (point B), the refrigerant is leaving in a superheated vapor state with a constant degree of superheating (ΔT_{sup}).
- The sensible heat transfer due to the refrigerant temperature change in the evaporator (from point A to point B) is neglected, as it is small compared to the latent heat transfer.
- The refrigerant leaves the condenser (point C) in a saturated liquid state.
- An isenthalpic expansion is considered through the electronic expansion valves (EEV).
- The pressure drop within the refrigerant pipes and the heat exchangers is neglected.

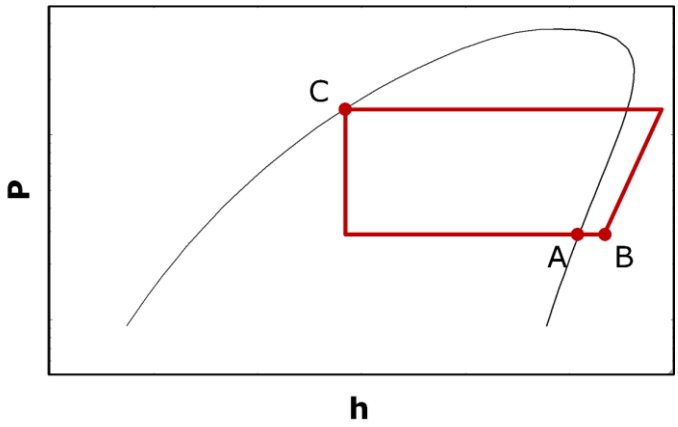

Figure 2. P-h diagram of the simplified vapor compression cycle.

The simplified cycle is a cornerstone for the flexibility of the new model. By considering only three thermodynamic states, such cycle has the benefit of lowering the computational time since limited refrigerant states need to be evaluated, including points A and C on the saturation lines. In contrast, existing VRF models that employ distributed parameter techniques like the finite volume method (Sun et al., 2017) and the moving boundary method (Cheung & Braun, 2014) demand a considerably larger number of refrigerant state evaluations. This disparity becomes particularly pronounced when applied to VRF systems featuring a substantial number of IUs. The use of the simplified cycle also plays a role in reducing the model parameters, thereby facilitating the parameter-estimation procedure. The VRF main components (i.e., the IUs and the OU) are modeled separately to ensure the model modularity, accommodating various configurations. Then, they are assembled according to the simplified cycle. A parameter-estimation procedure is used to evaluate the model parameters based on performance data provided by manufacturers.

The new VRF model considers the use of multiple compressors in parallel for large VRF systems. This allows for the variation in VRF capacity during part load operation to be accounted for, which is important since large VRF systems typically operate at less than 50% load throughout the year (Kibo, 2016). To properly manage the

start/stop signal of the compressors, an appropriate control strategy is required. A data-driven control strategy that uses a machine-learning algorithm to predict which compressors should turn on for a given set of operation conditions is developed by leveraging available manufacturer data.

2.2. Heat exchanger model

Considering an air-to-air VRF system, the indoor units (IUs) are likened to air-refrigerant heat exchangers (Figure 3) operating at a constant refrigerant temperature. During operation, the air-refrigerant heat exchanger may encounter moist air condensation, which leads to a wet coil surface. In this case, the coil outside surface is considered fully wet even if it is partially wet, as proposed by Braun et al. (1989). The total heat transfer of a wet coil and a dry coil can be described using the enthalpy potential method (McElgin & Wiley, 1940). This approach considers two parameters for the heat exchanger: the thermal conductance between the moist air and the coil surface (UA_c) and the thermal conductance between the refrigerant and the coil inside surface (UA_{ref}).

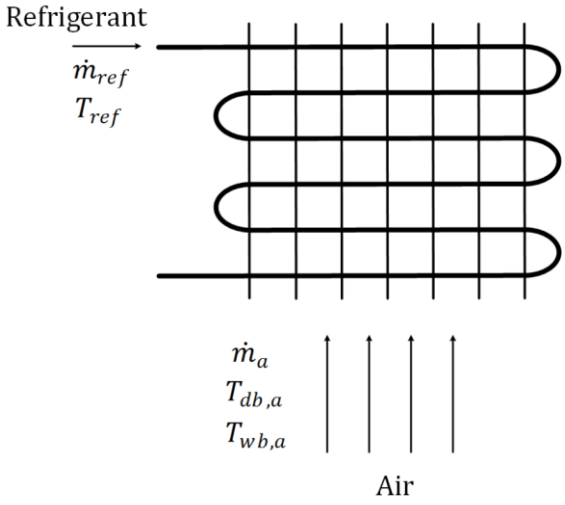

Figure 3. Schematic of the air-refrigerant coil.

From the enthalpy potential method, the coil total heat transfer rate ($\dot{q}$) is split into two parts: a sensible heat transfer rate ($\dot{q}_{sen}$) and latent heat transfer rate ($\dot{q}_{lat}$). The sensible heat transfer is accounted by considering the temperature difference between the air stream and a coil effective surface while the total heat transfer is accounted by considering the difference of air enthalpy at the inlet air conditions and at the refrigerant temperature. Using the effective surface temperature of the coil ($T_{c,eff}$), $\dot{q}_{sen}$ is evaluated by applying the ε-NTU method:

$$\dot{q}_{sen} = \varepsilon_{sen}\dot{m}_a c_{p,a}\left(T_{db,a} - T_{c,eff}\right) \quad (1)$$

$$\varepsilon_{sen} = 1 - e^{(-NTU_{sen})} \quad (2)$$

$$NTU_{sen} = UA_c/\dot{m}_a c_{p,a} \quad (3)$$

where ε_{sen} is the heat exchanger effectiveness for sensible heat transfer, NTU_{sen} is the number of transfer units for sensible heat transfer, $\dot{m}_a$ is the air mass flowrate, $c_{p,a}$ is the specific isobaric heat capacity of entering moist air and $T_{db,a}$ is the inlet air dry bulb temperature. $c_{p,a}$ is evaluated by considering the effect of humidity on the specific heat capacity:

$$c_{p,a} = (1 - X_a)c_{p,a,dry} + X_a c_{p,water} \quad (4)$$

$$X_a = f(T_{db,a}, T_{wb,a}) \quad (5)$$

where f refers to a thermodynamic state function, $T_{wb,a}$, X_a are the inlet air wet bulb temperature and the mass fraction of water in the air mixture, respectively, $c_{p,a,dry}$ is the specific isobaric heat capacity of dry air (i.e., 1006 J/kg.K), $c_{p,water}$ is the specific isobaric heat capacity of steam water (i.e., 1860 J/kg.K).

The effective surface temperature of the coil is also used to define the coil surface condition. When the effective surface temperature is below the dew point of the entering moist air ($T_{dp,a}$), condensation occurs at the coil surface, which results in a wet

coil regime. Conversely, the dry coil regime occurs when the coil effective surface temperature is above the dew point. However, for a given operation condition of a coil, the effective surface temperature is initially unknown. Its value is inferred from the corresponding specific enthalpy of saturated air ($h_{a,c,eff}$) by solving a non-linear system of equations that expresses the total heat transfer of the coil between the air stream and the effective surface:

$$\dot{q} = \varepsilon_{sen}\dot{m}_a\left(h_a - h_{a,c,eff}\right) \tag{6}$$

$$h_{a,c,eff} = \begin{cases} f\left(T_{c,eff}, X_a\right) & T_{c,eff} > T_{dp,a} \\ f\left(T_{c,eff}, X_{a,sat}\big|_{T=T_{c,eff}}\right) & T_{c,eff} \leq T_{dp,a} \end{cases} \tag{7}$$

$$h_a = f(T_{db,a}, T_{wb,a}) \tag{8}$$

where $X_{a,sat}$ is the saturated air humidity ratio and h_a is the enthalpy of the entering air.

The coil total heat transfer is also evaluated between the air stream and the refrigerant using a global heat transfer coefficient:

$$\dot{q} = \varepsilon\dot{m}_a\left(h_a - h_{a,ref}\right) \tag{9}$$

$$\varepsilon = 1 - e^{(-NTU)} \tag{10}$$

$$NTU = UA/\dot{m}_a c_{p,a} \tag{11}$$

$$UA = \frac{1}{\frac{1}{UA_c} + \frac{c_{p,a,c}}{c_{p,a}}\frac{1}{UA_{ref}}} \tag{12}$$

where UA is the global heat transfer coefficient between the air stream and the refrigerant, $c_{p,a,c}$ is the effective specific isobaric heat capacity of air that considers water condensation which corresponds to the change in enthalpy with respect to temperature along the saturation line, NTU and ε are the number of transfer units for the total heat transfer and the corresponding heat exchanger effectiveness, respectively and $h_{a,ref}$ is the enthalpy of moist air at the refrigerant temperature. The air properties are

evaluated for the following conditions:

$$h_{a,ref} = f(T_{ref}, X_{a,c}) \tag{13}$$

$$X_{a,c} = \begin{cases} X_a & T_{c,eff} > T_{dp,a} \\ X_{a,sat}\big|_{T=T_{ref}} & T_{c,eff} \leq T_{dp,a} \end{cases} \tag{14}$$

$$c_{p,a,c} = \begin{cases} c_{p,a} & T_{c,eff} > T_{dp,a} \\ \dfrac{dh_{a,s}}{dT}\Big|_{T=T_{ref}} & T_{c,eff} \leq T_{dp,a} \end{cases} \tag{15}$$

where T_{ref} is the refrigerant temperature, $X_{a,c}$ is the mass fraction of water in the air mixture at the coil surface conditions, $h_{a,s}$ is the enthalpy of saturated air. The derivative of saturated air enthalpy with respect to the temperature is approximated by finite differences considering a temperature difference (ΔT) of 0.1 °C:

$$\frac{dh_{a,s}}{dT}\Big|_{T=T_{ref}} = \frac{h_{a,s}\big|_{T_{ref}+\Delta T} - h_{a,s}\big|_{T_{ref}}}{\Delta T} \tag{16}$$

Knowing the total and the sensible heat transfer of the coil, the latent heat transfer rate ($\dot{q}_{lat}$) is evaluated by an energy balance:

$$\dot{q}_{lat} = \dot{q} - \dot{q}_{sen} \tag{17}$$

In heating mode, when the heat exchanger operates as a condenser, the coil effective surface temperature is always higher than the dew point of the moist air. As a result, the latent heat transfer rate becomes zero since the coil surface is fully dry.

2.3. Compressor model

It is assumed that the VRF system operates using a scroll compressor. As proposed by Winandy et al. (2002), a scroll compressor mechanical work can be modeled as a result of two successive processes: (1) an isentropic compression at the built-in volume ratio and (2) an isochoric compression to the discharge pressure:

$$\dot{W}_t = \frac{\gamma}{\gamma - 1} p_{eva} \dot{V}_{nom} \left(\frac{\gamma}{\gamma - 1} \frac{p_{con}}{p_{eva} V_r} + \frac{1}{\gamma} p_r^{\frac{\gamma}{\gamma - 1}} - 1 \right) \quad (18)$$

where $\dot{W}_t$ is the theoretical compressor work, p_{eva} and p_{con} are the evaporating and condensing pressures, $\dot{V}_{nom}$ is the nominal volume flow rate at the compressor suction, γ is the isentropic exponent of the refrigerant evaluated at the compressor suction (i.e., at $T = T_{eva} + \Delta T_{sup}$ and $p = p_{eva}$), V_r is the compressor built-in volume ratio between the discharge and the suction and $p_r = V_r^{\gamma}$ is the built-in pressure ratio.

The compressor power input is given by:

$$\dot{W} = \frac{\dot{W}_t}{\eta} + \dot{W}_{loss} \quad (19)$$

where η is the compressor electromechanical efficiency and $\dot{W}_{loss}$ are constant power losses.

The refrigerant mass flowrate is evaluated by considering a leakage flow rate, as proposed by Chen et al. (2000):

$$\dot{m}_{ref} = \frac{\dot{V}_{nom}}{v_{suc}} - C \frac{p_{con}}{p_{eva}} \quad (20)$$

where v_{suc} is the refrigerant specific volume evaluated at the compressor suction and C is the leakage coefficient.

2.4. VRF model and implementation

The VRF system model is composed of several IUs and OUs. The IU model represents the heat exchanger model while the OU model includes a heat exchanger and one or more scroll compressors. These models are connected based on the simplified vapor compression cycle. For a VRF system with multiple compressors, the total power input ($\dot{W}_{VRF}$) is given by the sum of the power inputs of all compressors:

$$\dot{W}_{VRF} = \sum_i \frac{\dot{W}_t^{(i)}}{\eta^{(i)}} + \dot{W}_{loss}^{(i)} \tag{21}$$

where i represents the compressor index.

The total evaporator heat transfer rate ($\dot{q}_{eva}$) is evaluated from the enthalpy difference of the refrigerant between points A and C:

$$\dot{q}_{eva} = \dot{m}_{ref,VRF}(h_A - h_C) \tag{22}$$

$$\dot{m}_{ref,VRF} = \sum_i \left(\frac{\dot{V}_{nom}^{(i)}}{v_{suc}} - C^{(i)} \frac{p_{con}}{p_{eva}} \right) \tag{23}$$

where $\dot{m}_{ref,VRF}$ is the total refrigerant mass flowrate of the VRF system.

The total condenser heat transfer rate, $\dot{q}_{con}$, is obtained by an energy balance:

$$\dot{q}_{con} = -(\dot{q}_{eva} + \dot{W}_{VRF}) \tag{24}$$

The total heat transfer rates of the evaporator ($\dot{q}_{eva}$) and the condenser ($\dot{q}_{con}$) are linked to the heat transfer rates of the individual units following their operation mode. For instance, in cooling mode, all IUs operate as evaporators, while the OU operates as a condenser. Therefore, the heat transfer rates $\dot{q}_{eva}$ and $\dot{q}_{con}$ are given by:

$$\dot{q}_{eva} = \sum_i \dot{q}_{IU}^{(i)} \tag{25}$$

$$\dot{q}_{con} = \dot{q}_{OU} \tag{26}$$

where $\dot{q}_{OU}$ is the heat transfer rate of the OU and $\dot{q}_{IU}^{(i)}$ is the heat transfer rate of the i-th IU.

The IU and the OU models are implemented in Modelica based on the Modelica IBPSA library (Wetter et al., 2015). Modelica features acausal and object-oriented modeling for large and complex physical systems. Its particularity in HVAC system modeling has been well documented (P. Li et al., 2014). The object-oriented approach

facilitates model reuse and extension. For a VRF heat pump system, its model is derived from the combination of an OU model and several IU models. As the implementation is vector-based, the VRF model can support a large number of IUs and OUs. The simulation of the VRF system is achieved by solving a nonlinear system of equations formed through the integration of component models. The heat exchanger and compressor models are interconnected through specific variables, namely, the refrigerant saturation pressure at both the condenser (p_{con}) and evaporator (p_{eva}), as well as the total refrigerant mass flowrate ($\dot{m}_{ref,VRF}$). The inputs required for the final VRF simulation model are the dry bulb temperature, the wet bulb temperature and the return air mass flowrate of the zones, as well as the outdoor air temperature, humidity ratio, and mass flowrate.

3. Parameter-estimation procedure

The VRF model has several parameters that need to be specified. For the IU model, the heat exchanger parameters are the two thermal conductance (UA_c and UA_{ref}). The OU model heat exchanger has the same parameters (UA_c and UA_{ref}) while each of its compressors has 6 parameters ($\dot{V}_{nom}$, V_r, C, η, $\dot{W}_{loss}$ and ΔT_{sup}). These parameters are unknown for commercial VRF units because the manufacturers do not disclose such information. The proposed approach is to estimate these parameters by calibration using the units' performance data provided by the manufacturers. Such information is typically included in the product data sheets in the form of performance tables. For IUs, available data include the latent and sensible capacities at different air flow rates and temperatures (dry bulb and wet bulb). For OUs, manufacturers provide the total capacity at different system combination ratios and airflow temperatures in addition to the VRF power consumption, which includes the compressors and the outdoor fan

motor power inputs. The combination ratio (CR), also known as the capacity index, is defined by:

$$CR = \frac{\sum_i \dot{q}_{nom,IU}^{(i)}}{\dot{q}_{nom,OU}} \tag{27}$$

where $\dot{q}_{nom,OU}$ is the nominal capacity of the OU and $\dot{q}_{nom,IU}^{(i)}$ is the nominal capacities of the i-th IU.

The proposed calibration method is a macro parameter estimation procedure as defined by Reddy (2006). This approach aims to infer overall or aggregate parameters from reference data such as manufacturer data. Parameters are obtained by minimizing a cost function based on the error between the model simulation results and the reference data. Calibration routines using the Modelica based IU and OU component models are implemented in Python. The Sequential Least Squares Programing method (SLSQP) from the Python SciPy library (Virtanen et al., 2020) is used as the optimization algorithm and the convergence tolerance is set to 10^{-6}.

3.1. Indoor unit model calibration

The calibration procedure for the IU model is illustrated in Figure 4. The model inputs are the entering air mass flowrate, dry bulb temperature, wet bulb temperature and the total capacity while the computed outputs are the sensible and latent capacities.

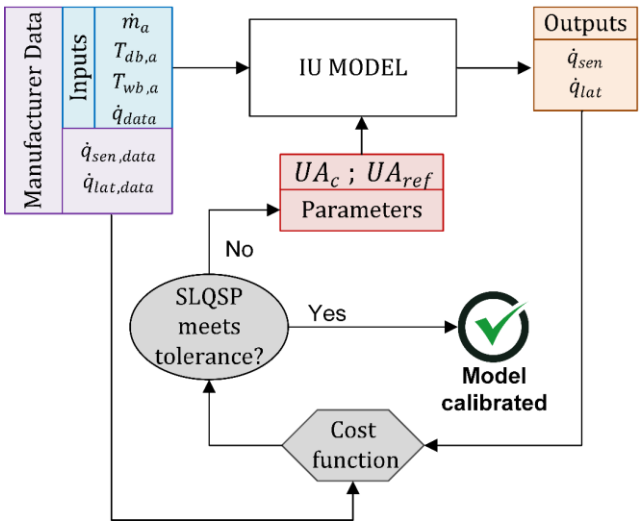

Figure 4. Indoor unit calibration procedure.

The cost function associated to the IU model calibration is:

$$SSE_{IU} = \sum_j \left[\left(\frac{\dot{q}_{sen} - \dot{q}_{sen,data}}{\dot{q}_{sen,data}} \right)^2 + \left(\frac{\dot{q}_{lat} - \dot{q}_{lat,data}}{\dot{q}_{lat,data}} \right)^2 \right] \tag{28}$$

where for the data points (j): $\dot{q}_{sen}$ and $\dot{q}_{lat}$ are the IU model sensible and latent capacities, $\dot{q}_{sen,data}$ and $\dot{q}_{lat,data}$ are the latent and the sensible capacities from the IU manufacturer data. It is important to choose proper guess values to facilitate the convergence of the parameters.

A guess value selection procedure based on the nominal value of the capacity is proposed:

$$UA^{guess} = \frac{\dot{q}_{nom,IU}}{\Delta T} \tag{29}$$

$$UA_c^{guess} = UA^{guess} \cdot (r+1) \tag{30}$$

$$UA_{ref}^{guess} = UA^{guess} \cdot \frac{(r+1)}{r} \tag{31}$$

where ΔT is the heat exchanger pinch and r is the ratio between airside and refrigerant-side convective heat transfer coefficient. Values of 15 K and 0.5 have been considered for ΔT and r respectively.

3.2. Outdoor unit model calibration

A VRF OU may include several heat exchangers and compressors. However, the size of each single component is usually unknown. Manufacturers provide information about the OU total capacity, which considers the contribution of each heat exchanger. The number of compressors installed in the OU is also usually provided. Some manufacturers release more information by detailing the volume flow rate ($\dot{V}_{nom}$) of each compressor but their activation order is always missing as most systems perform compressor duty cycling.

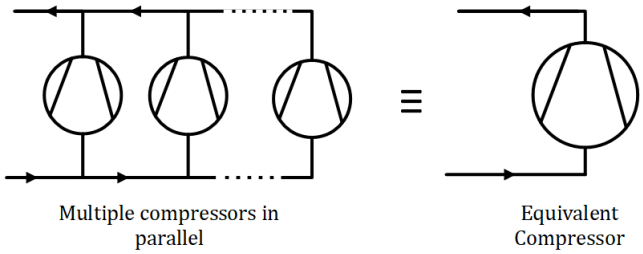

Figure 5. Compressor equivalence for the OU model calibration.

To address the shortcomings in the OU setup information for the calibration procedure, it is assumed that the model includes one heat exchanger, and all compressors have the same size. This assumption helps to ease the OU calibration by considering one equivalent compressor as shown in Figure 5. Since the compressors operate at the same pressure ratio, as they are in parallel, it is considered they have the same built-in volume ratio, electromechanical efficiency, and superheating degree as the equivalent compressor (Equation 32). The remaining parameters are different between each of them. From the calibration results, single compressor parameters are evaluated by:

$$\left\{V_r^{(i)}, \Delta T_{sup}^{(i)}, \eta^{(i)}\right\} = \left\{V_r^{cal}, \Delta T_{sup}^{cal}, \eta^{cal}\right\} \tag{32}$$

$$\left\{\dot{V}_{nom}^{(i)}, \dot{W}_{loss}^{(i)}, C^{(i)}\right\} = \left\{\frac{\dot{V}_{nom}^{cal}}{N}, \frac{\dot{W}_{loss}^{cal}}{N}, \frac{C^{cal}}{N}\right\} \quad (33)$$

where cal refers the calibrated values and N is the number of compressors.

The OU calibration model involves an equivalent compressor and a single heat exchanger. To determine its capacity and power input, an IU is added to the calibration model (Figure 6) to complete the thermodynamic cycle. The parameters of the additional IU are also calibrated during the process. While the manufacturer data provides all necessary inputs for the load side heat exchanger, temperatures are the only available data on the source side. For instance, in cooling mode, the available evaporator data are the dry bulb temperature ($T_{db,a,eva}$), the wet bulb temperature ($T_{wb,a,eva}$) and the air mass flowrate ($\dot{m}_{a,eva}$) while for the condenser, only the dry bulb temperature ($T_{db,a,con}$) is known. To complete the inputs data of the calibration model, the condenser air flowrate is assumed to be the same as for the evaporator and a constant relative humidity of 50% is considered. The heat transfer of the additional IU (i.e., $\dot{q}_{con}$ in cooling mode) is not included in the calibration cost function, even if its parameters are calibrated, as it is not a part of the calibrated OU model. Therefore, the sum of squared errors for the OU calibration model (SSE_{OU}) is based solely on the evaporator capacity ($\dot{q}_{eva}$) and the VRF power input ($\dot{W}_{VRF}$) and is given by:

$$SSE_{OU} = \sum_{j}\left[\left(\frac{\dot{q}_{eva} - \dot{q}_{eva,data}}{\dot{q}_{eva,data}}\right)^2 + \left(\frac{\dot{W}_{VRF} - \dot{W}_{VRF,data}}{\dot{W}_{VRF,data}}\right)^2\right] \quad (34)$$

where for the set of data points (j): $\dot{q}_{eva}$, $\dot{W}_{VRF}$, $\dot{q}_{eva,data}$ and $\dot{W}_{VRF,data}$ are the capacity and the power consumption respectively evaluated by the model and from the manufacturer data. To evaluate the cost function, only data in full load operation with a combination ratio of 100% is considered. Similar to the IU calibration procedure, a

sequence that evaluates the compressor guess values is implemented, based on the OU nominal performances and the rated condition. More details on this sequence can be found in (Mbaye & Cimmino, 2021).

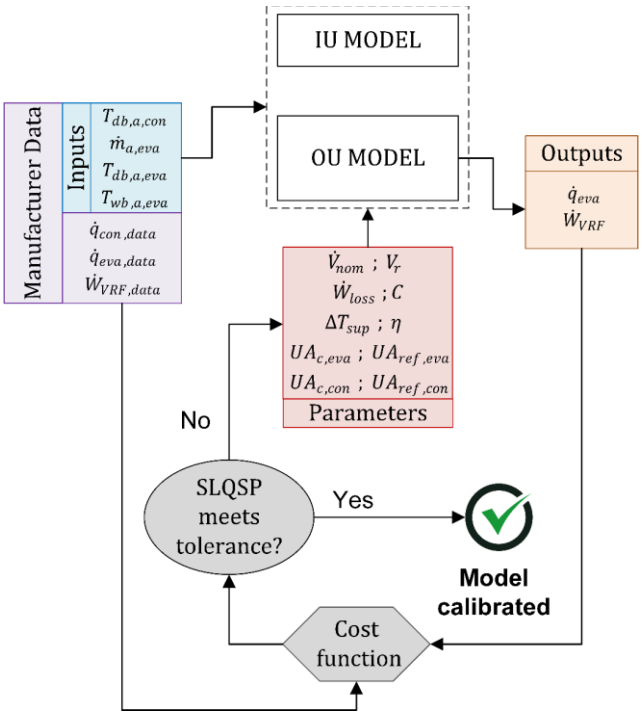

Figure 6. OU calibration procedure for cooling mode operation.

4. Control strategy

Large size VRF systems for large building applications usually contain multiple compressors for capacity variation to meet the IU demands. In some commercial units, the capacity controller allows a variation range from 6% to 100% using multiple single-speed compressors. At the start of the operation, only one compressor is running while the others are turned off or are in standby mode. When the IUs thermal demand increases due to a variation of the setpoint temperature or to an increase of the number of active units, other compressors start working to meet the system's load. Thus, the VRF model must have a capacity controller to select the correct number of compressors to run for a given operation condition. Several authors (Elliott & Rasmussen, 2009;

Xiangguo et al., 2013; H. Yan et al., 2016; Zhu et al., 2015) have proposed VRF capacity control strategies but very few of them focused on systems with multiple compressors. The only known work that enters this category is the control method proposed by Tu et al. (2016). However, their method applies to systems with variable speed compressors and needs the knowledge of some of the system's internal characteristics such as the suction pressure control target.

The proposed VRF control strategy aims to select the proper number of compressors that balances the IU demands. It applies to systems that are equipped with single-speed compressors. Since the operational characteristics of commercial units are typically not accessible, the capacity controller relies on information contained in the manufacturer's data.

4.1. Capacity control method

The first step in the development of the VRF model control strategy is to identify the key operation variables that affect the system's capacity and power consumption. For traditional heat pumps, as presented by the DOE2 model (Hydeman & Gillespie, 2002), the capacity is a function of two main variables: the condenser fluid entering temperature and the evaporator fluid entering temperature. The same approach applies to VRF systems (Raustad, 2013) where the capacity depends on the combination ratio, in addition to the IU average dry bulb temperature and the OU dry bulb temperature. The simplified vapor compression cycle considers only two temperature levels: one evaporation temperature and one condensation temperature. From that, when the IUs have different entering air temperatures, the VRF capacity is more affected by the IU with the most extreme temperature. In cooling mode, it corresponds to the lowest IU temperature and, to the highest IU temperature, in heating mode.

In order to design the controller, a compressor map that indicates the number of compressors required to achieve the desired capacity is generated based on available data. The approach consists of, for each operational condition, simulating the previously calibrated VRF model using every possible number of compressors. Then, the optimal number of compressors for these conditions is the one that minimizes the error between the model output and the data.

The compressor map can be generated using both manufacturer data and measured data. Manufacturers provide data on the VRF capacity for specific combination ratios, as well as the IU and OU dry bulb temperatures. For a given operational condition (j) in the manufacturer data, the optimal number of compressors ($nCom$) is the one that minimizes the error between the predicted capacity ($\dot{q}$) and the capacity provided by the manufacturer ($\dot{q}_{data}$):

$$nCom_{data}^{(j)} \equiv \min\left[\frac{|\dot{q} - \dot{q}_{data}|}{\dot{q}_{data}}\right] \tag{35}$$

The same approach can be used to generate the compressor map based on measured data. When the VRF system capacity and the IU activation are recorded, the combination ratio is evaluated using Equation 27 and the compressor map is generated using Equation 35. In the case where the VRF power consumption is measured instead of the capacity, the optimal number of compressors is evaluated by:

$$nCom_{mes}^{(j)} \equiv \min\left[\frac{|\dot{W}_{VRF} - \dot{W}_{mes}|}{\dot{W}_{mes}}\right] \tag{36}$$

where for the operational condition (j) $\dot{W}_{VRF}$ is the model's power and $\dot{W}_{mes}$ is the system's measured power.

4.2.Controller design

An analysis of the compressor map reveals a lack of clear patterns, suggesting that the

relationship between variables is more intricate than previously assumed. To achieve precise and adaptable control of the VRF system, the capacity controller is implemented using a machine learning algorithm. This approach offers several advantages over traditional methods, including the ability to effectively capture complex relationships between multiple variables, such as OU and IU temperatures, and combination ratios. Additionally, the algorithm can be trained with a wide range of data sources, including data collected from field tests and during both heating and cooling mode. Predicting the number of working compressors from a compressor map can be viewed as a classification task in the context of machine learning. In other words, the objective is to classify the number of compressors required based on the operating conditions. The decision tree learning method was chosen to solve the compressor map classification problem due to its white box model nature. Compared to other machine learning classifiers, decision trees provide a set of rules expressed through Boolean logic that can be easily interpreted.

The Python Scikit-learn library (Pedregosa et al., 2011) is used to develop the decision tree model. To avoid overfitting, the model maximum depth is set to the number of classes (i.e., the number of working compressor) minus one. The accuracy of the overall classification model is determined using the accuracy score, which is calculated as follows:

$$Accuracy = \frac{1}{n} \sum_{i=0}^{n-1} 1\ (if\ \hat{y}_i = y_i) \tag{37}$$

where n is the number of samples, $\hat{y}_i$ is the predicted value of the i-th sample and y_i is its corresponding true value. To evaluate the model's ability to predict each class independently, precision, recall, and F1-score metrics are used. These metrics are defined as follows:

$$Precision = \frac{\left|Y_L \cap \hat{Y}_L\right|}{\left|\hat{Y}_L\right|} \tag{38}$$

$$Recall = \frac{\left|Y_L \cap \hat{Y}_L\right|}{\left|Y_L\right|} \tag{39}$$

$$F1 - Score = 2\frac{Precision \times Recall}{Precision + Recall} \tag{40}$$

where for a class L and for given testing data samples, Y_L is the set of true values and $\hat{Y}_L$ set of predicted values. The data samples are split into 80% for training and 20% for testing, and the decision rules obtained from the trained model are implemented in Modelica.

5. Model validation

5.1. ASHRAE headquarters building data

The VRF heat pump model including its control strategy is validated using data obtained from the HVAC systems installed in the former ASHRAE Headquarters Building located in Atlanta (USA). The ASHRAE VRF system serves the first floor of the building, which includes office areas and conference rooms. It consists of two outdoor heat recovery units, each with a cooling capacity of 49 kW. The OUs are equipped with four compressors each, resulting in a total of eight compressors for the entire VRF system. The system also includes 22 ducted indoor units of various capacities, which are connected to a 3-pipe heat recovery system and operate at a constant airflow rate when the IU is on. The HVAC system also features a dedicated outdoor air system (DOAS), which supplies fresh air to the thermal zones.

The ASHRAE HQ building is a "living laboratory" and is highly instrumented, particularly with respect to the HVAC system, with operating data such as indoor and outdoor temperatures, setpoints, and power usage being measured and recorded. A

comprehensive description of the building HVAC system, control strategies, and performance can be found in the studies by Southard et al. (2014a, 2014b). Measured data from the VRF system were collected over two years of operation, from July 1, 2011, to June 30, 2013, and included zone dry bulb temperature, individual unit operating status, operating mode, airflow rate, discharge air temperature, total VRF electric power use, and outdoor air temperature. Additionally, engineering data, manufacturer operation and installation manuals for all the equipment models in the HVAC system are available. Data for airflow rate, zone temperature, and discharge temperature are recorded at 15-minute intervals, while data for operating mode, operating status, and occupation status are recorded when they change. Data on the total electric power used by the VRF system and the outdoor air temperature are collected every 5 minutes.

The collected data include the VRF system operation in heating dominant and cooling-only modes but do not cover the heating-only mode. In the heating-dominant mode, while most zones require heating, there are still some zones with cooling demands. Consequently, the VRF system operates in a heat recovery mode, providing both heating and cooling simultaneously. However, it is important to note that the proposed model considers only single-mode operation, either heating or cooling. Therefore, the measured data from instances where the system operates in heat recovery mode cannot be utilized. Consequently, the validation of the model will be conducted exclusively in the cooling mode. The validation period spans 60 days from July 1, 2011, to August 29, 2011, during which the ASHRAE VRF system operated solely in cooling mode.

5.2. VRF system calibration

The ASHRAE VRF model parameters are determined using manufacturer data. The

VRF system comprises 22 IUs of seven different types, with the parameters of each type estimated through the parameter-estimation procedure. Since the focus of the study is on cooling mode, the model parameters are evaluated for cooling operation only. Table 1 presents the calibration results for the 7 IU types, including the operating mass flow rate in cooling mode and the coefficient of the variation of the root mean square error (CVRMSE) for the latent and sensible capacities. A notable observation from the calibration results of the IU is that the CVRMSE related to the latent capacity of the IU with a nominal capacity of 2.05 kW is significantly higher compared to the other IU. While all these indoor units are ceiling-mounted models equipped with a Sirroco-type fan, the 2.05 kW IU stands out as the only wall-mounted model featuring a crossflow fan. This distinct fan configuration could potentially lead to variations in heat transfer characteristics. A potential scale effect may also be considered, where the CVRMSE of smaller-sized units appears to be more influenced. Figure 7 shows the comparison between the predicted values and the manufacturer data for the sensible and latent capacities for the IU type of 8.8 kW nominal capacity.

Table 1: IUs calibration results

Nominal Capacity [kW]	Number of IUs	Nominal Flowrate [l/s]	UA_c [W/K]	UA_{ref} [W/K]	CVRMSE ($\dot{q}_{sen}$) [%]	CVRMSE ($\dot{q}_{lat}$) [%]
2.05	1	122.7	383	582	5.5	19.2
3.52	9	160.5	301	692	2.6	4.2
5.28	6	250.1	424	1270	3.0	4.9
7.03	1	349.2	614	1178	3.3	5.9
8.80	2	325.6	485	1193	3.0	4.0
10.55	2	481.2	896	2069	3.5	5.8
14.07	1	599.4	1316	1454	3.1	4.9

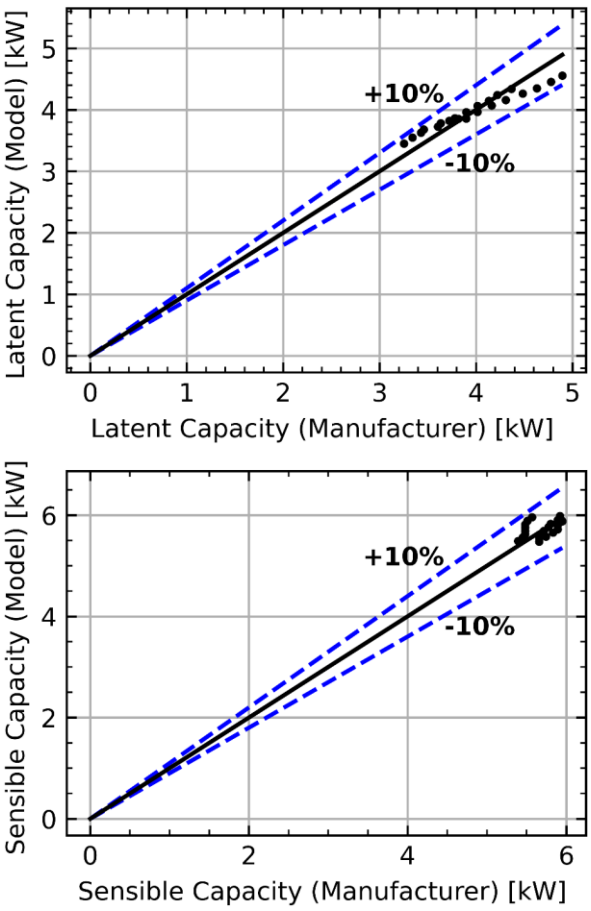

Figure 7. Comparison between the manufacturer data and the simulation results for an IU of 8.8 kW nominal capacity: latent capacity (top), sensible capacity (bottom).

In cooling operation, the heat exchangers of the two OUs function as condensers, and the global thermal conductance of the coil as well as the parameter of each of the eight compressors was calibrated. Table 2 displays the OUs parameters obtained after calibration and Figure 8 illustrates the comparison between the predicted and manufacturer values for the total capacity and power input. The calibration results CVRMSE is 1.4% and 1.8% for the power input and total capacity, respectively.

Table 2: OU parameters obtained after calibration.

Parameters	Values
UA_c $[W/K]$	14767
UA_{ref} $[W/K]$	29534
Number of compressors	8
Value per compressor	

$\dot{V}_{nominal}\ [m^3/s]$	17.15e-4
$V_r\ [-]$	2.64
$C\ [kg/s]$	9.4e-4
$\eta\ [-]$	0.7
$\dot{W}_{loss}\ [W]$	6.4
$\Delta T_{sup}\ [°C]$	0.5

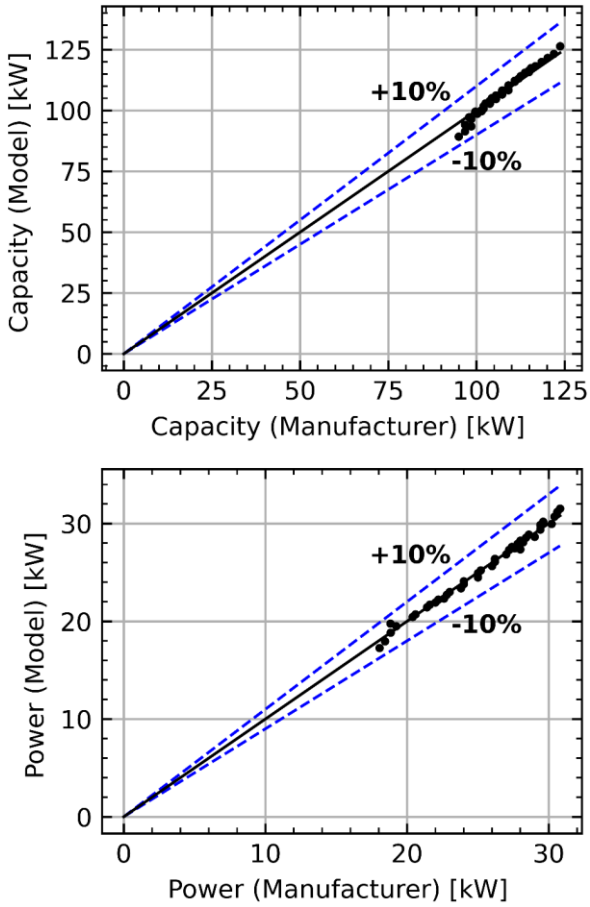

Figure 8. Comparison between the manufacturer data and the simulation results for the OUs: Total capacity (Top), Power consumption (Bottom).

5.3. Controller tuning

The tuning of the controller decision rules can be achieved using manufacturer data. The provided data cover a range of combination ratios from 50% to 130%, which is too high to include operation with only one compressor. To ensure that all compressor classes are represented, artificial data is generated for a combination of 5% assuming

that only one compressor is operating for all temperatures. The compressor map generated from the manufacturer data is presented in Figure 9, which is then used to train the decision tree model. As the VRF system has eight compressors, the maximum depth of the decision tree is set to 7. The overall accuracy of this data-tuned controller prediction is 72%, and the corresponding scores for each compressor class are detailed in Table 3.

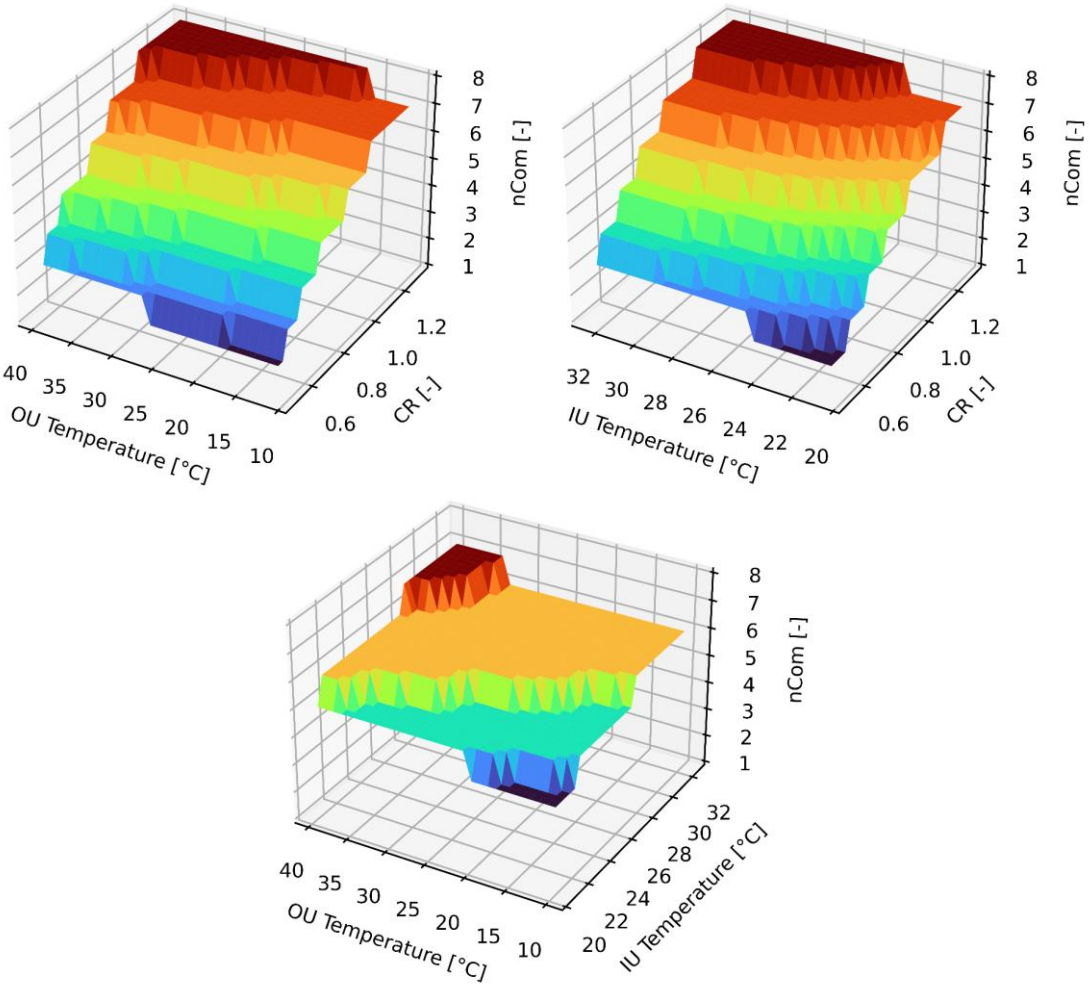

Figure 9. Compressor map generated using the manufacturer data.

Table 3: Decision tree prediction score for the data-tuned controller.

Class	*Precision*	*Recall*	*F1-Score*
1	1	1	1
2	0.67	0.67	0.67
3	0.82	0.75	0.78

4	0.66	0.74	0.7
5	0.41	0.61	0.49
6	0.59	0.36	0.44
7	0.57	0.33	0.42
8	0.85	0.94	0.89

An alternate controller model is also trained with the measured data from the building VRF system. As the VRF capacity is not recorded, the compressor map is generated based on the VRF power consumption using data recorded for 6 weeks of operation. The resulting accuracy of the measurement-tuned controller prediction is 76% and Table 4 provides detailed scores for each compressor class.

Table 4: Decision tree prediction score for the measurement-tuned controller.

Class	*Precision*	*Recall*	*F1-Score*
1	0.76	0.79	0.77
2	0.29	0.21	0.24
3	0.59	0.69	0.63
4	0.68	0.72	0.7
5	0.71	0.67	0.69
6	0.57	0.57	0.57
7	0.62	0.54	0.58
8	0.78	0.8	0.79

5.4. Validation procedure

To verify the accuracy of the model, the VRF system is simulated in cooling mode using the recorded operating conditions of the building. The manufacturer data-tuned controller is utilized for this operation. The simulation period includes, during certain late-night weekends, some brief moments when all the IUs are turned on simultaneously. This seems to be due to maintenance of the VRF system. These moments are excluded from the results analysis because they do not accurately represent the typical operation of the system.

In order to evaluate the effectiveness of the control method, the measurement-tuned controller is also used to simulate the VRF system. Since the training sample

consists of data recorded during six weeks out of the eight-week simulation period, the system is simulated for the remaining two weeks of the simulation period.

The VRF model simulation requires various inputs such as outdoor air temperatures, OU airflow rates, return air temperatures, and flow rates to each zone. In the building's thermal zones, only zone temperatures and discharge air temperatures are recorded, which may differ from the required input of return air temperature. In eight of the zones, fresh air is supplied directly from the DOAS, resulting in the return air being entirely made up of the zone air. However, in the remaining zones, the fresh air from the DOAS mixes with the return air supplied to the IUs, posing a challenge in determining the exact return air temperature. Southard et al. (2014b) conducted previous research to estimate the return air temperature and found that it was on average 1.6 ℃ lower than the zone temperatures. However, due to significant data scatter, a reliable correlation could not be established. Consequently, the assumption was made that the return air temperature is equivalent to the measured zone temperatures for all zones. The VRF simulation model also requires zone humidity as an input, but none of the thermal zones has recorded data for this parameter. As a result, a return air relative humidity of 50% is set for all IUs, following the recommendation from ASHRAE Standard 55 for an operative temperature between 23°C and 26°C in cooling.

Southard et al. (2014b) additionally performed an intricate uncertainty analysis on the measurements, considering the precision of the instruments employed. Their findings indicated that the uncertainties linked to key measurements are as follows:

- The return air temperature of the zones and the outdoor air temperature are gauged using sensors with a manufacturer-stated accuracy of ±0.2°C.
- The measurements of the airflows for both the indoor unit (IU) and the outdoor unit (OU) carry uncertainties rated at ±11.5%.

- The uncertainties related to measuring the electricity consumption of the VRF system are comparatively negligible when contrasted with the uncertainties affecting the other measured quantities.

To evaluate the accuracy of the model, it is necessary to establish a validation criterion. In the building energy performance simulation (BEPS) community, standardized statistical indices have been adopted to measure the discrepancy between simulated and measured data (Coakley et al., 2014). These indices, such as the normalized mean bias error (NMBE) and the coefficient of variation of the root mean square error (CVRMSE), are often used.

$$NMBE = \frac{1}{\overline{m}} \frac{\sum_{i=1}^{n}(m_i - s_i)}{n} \cdot 100(\%) \tag{41}$$

$$CVRMSE = \frac{1}{\overline{m}} \sqrt{\frac{\sum_{i=1}^{n}(m_i - s_i)^2}{n}} \cdot 100(\%) \tag{42}$$

ASHRAE Guideline 14 (ASHRAE, 2014) has provided guidelines for the limits of these indices for models that have been calibrated using hourly and monthly data (Table 5). However, there are currently no specific limits available in ASHRAE guidelines for daily data. To address this issue, Robertson et al. (Robertson et al., 2013) proposed acceptable limits for daily calibrated simulations by interpolating between the monthly and hourly criteria. They suggested that, for daily energy usage, a model is considered calibrated when the NMBE and CVRMSE are both below 6% and 18%, respectively. These different limits are used as the criteria for assessing the performance of the VRF model.

Table 5: Criteria limits for the validation of calibrated models.

Time scale	CVRMSE [%]	NMBE [%]
Hourly	30	10
Daily	18	6
Monthly	15	5

5.5. Results

The VRF power consumption during the cooling period is compared to simulation results, and Figure 10 illustrates the comparison results for a selected week. This week is chosen as the third week of the simulation period, spanning from July 17 to July 22, 2011. It is worth noting that this week also coincides with a period where the daily relative error between the measured and simulated VRF energy is at its lowest. The results show a good agreement between the measured and simulated data, and the capacity controller effectively captures the load variations. The number of compressors adjusts according to the operational conditions, ranging from a single compressor for very low loads to up to eight compressors for full-load operation. However, there are some instances where the predicted number of compressors is inaccurate, resulting in a significant discrepancy between the measured and simulated power consumption. This trend remains for the entire cooling period. The error in predicting the number of compressors can be attributed to the inherent bias present in the manufacturer data considered for tuning the controller. This data tends to favor a higher number of compressor operations, as it does not include operations with low combination ratios (below 50%). Also, the ASHRAE VRF system; given its specific characteristics including the number of IUs, the piping configuration and the control applied; operates differently from the standard system represented by the manufacturer data. Consequently, the two systems exhibit variations in their instantaneous behavior that lead to differences in their power profiles.

Figure 11 illustrates the evaluation of daily energy consumption, revealing a broad distribution of the relative error between the simulation results and measurements. The error ranges from 0.1% to 60%, indicating a wide scattering of results. However, for the entire cooling period, the relative error between the VRF's

total energy consumption and the measured energy reduces significantly, dropping to less than 1%.

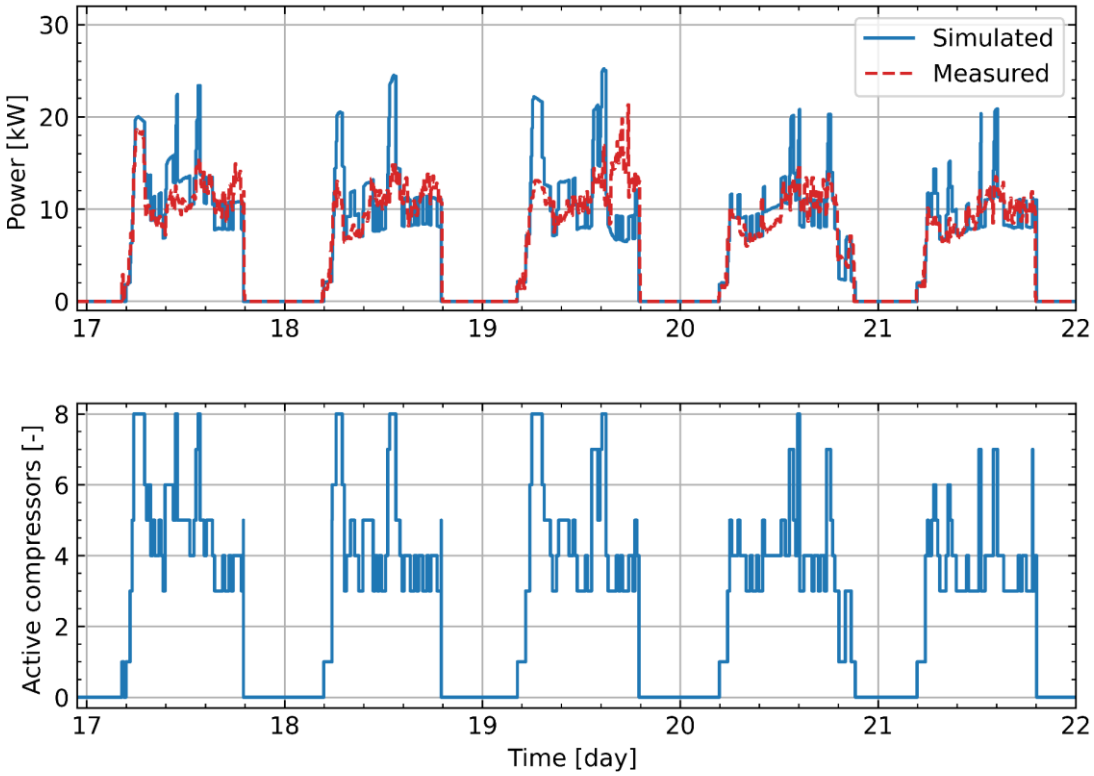

Figure 10. Comparison between measured and simulated VRF power for the selected week (Top). Number of working compressors (Bottom).

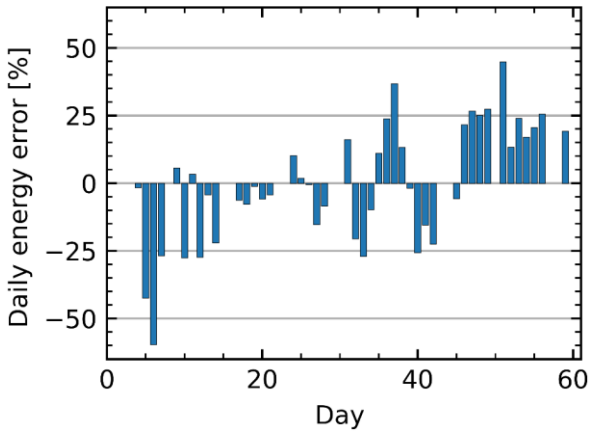

Figure 11. Daily relative error between measured and simulated VRF energy.

Table 6 provides an overview of the statistical errors obtained from the comparison of the simulation results and the measurements for both a daily time scale and an hourly time scale. The analysis of the hourly data indicates that the CVRMSE and the NMBE are 24% and 0.4%, respectively. If the data collected during system maintenance periods, which are considered to be outliers, are excluded from the analysis, then the resulting CVRMSE and NMBE values become 22.7% and 1%, respectively. The results obtained from both the inclusion and exclusion of outlier data are within the ASHRAE guidelines acceptable limits. When comparing the results on a daily time scale, the limits set by Robertson et al. (2013) for CVRMSE and NMBE remain applicable both with the inclusion and exclusion of outlier data.

Table 6. Statistical errors from the comparison results.

Quantity	Indices	Model	
		With outliers	Without outliers
Power (1h)	CVRMSE [%]	24	22.7
	NMBE [%]	0.4	1.0
Daily Energy	CVRMSE [%]	18.2	16.7
	NMBE [%]	0.4	1.6

The simulation results from the two different controllers, one tuned using manufacturer data and the other using measured data, are compared over a selected test period. To uphold a balanced 20%-80% split between training and testing data, a two-week interval is designated as the test period. The remaining weeks, which amount to six weeks, are employed for training the measurement-tuned controller given that the collected data spans eight weeks. Furthermore, the training period is divided into two segments. The two-week test period is bounded by the two segments of the training period. This prevents extrapolating on the system's characteristics by ensuring that the extreme operating temperatures are included in the training period.

The performance of the two controllers is assessed based on the power consumption and number of compressors used by the VRF system, as shown in Figure 12 and Figure 13. The results indicate that the measurement-tuned controller was able to better capture load variations, resulting in good agreement between the simulated and measured power consumption. Conversely, the data-tuned controller tends to overestimate the number of working compressors, leading to higher VRF power consumption. These findings are supported by the error analysis presented in Table 7, which shows that the measurement-tuned controller outperforms the data-tuned controller in terms of CVRMSE and NMBE, even when accounting for outliers. Nevertheless, both controllers' results are found to be within the acceptable range defined by ASHRAE guidelines.

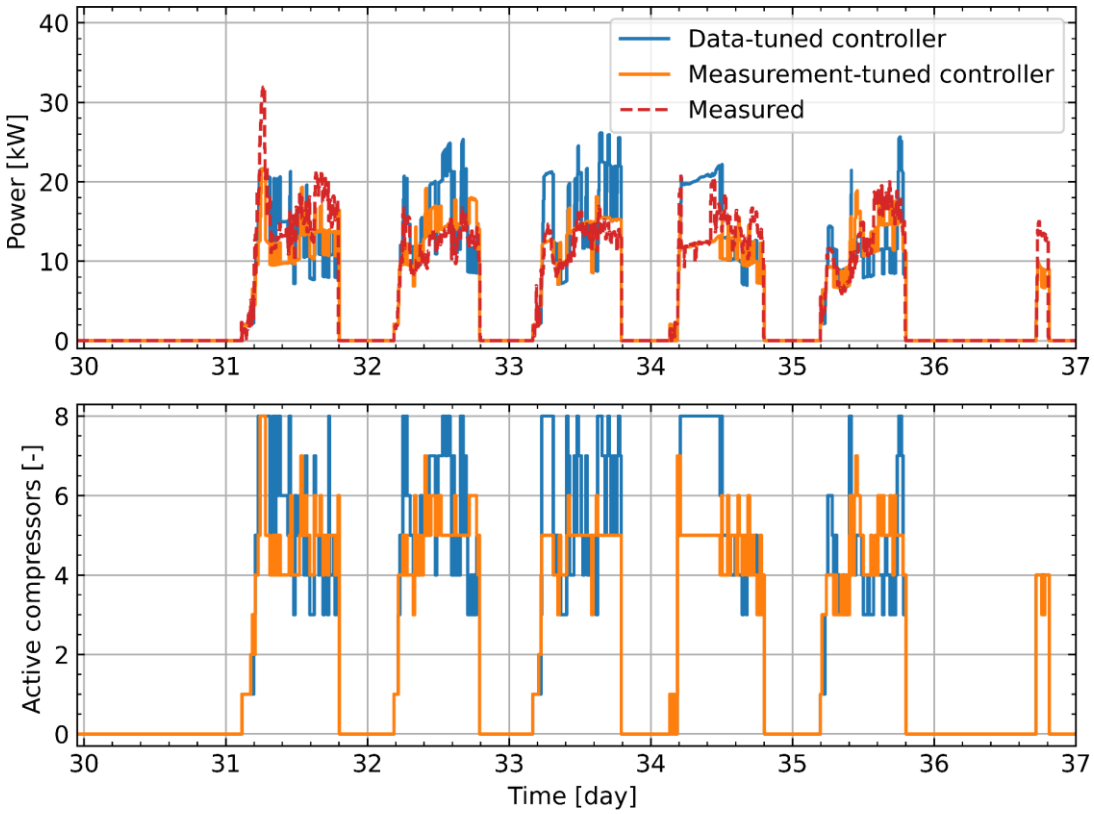

Figure 12. Comparison results between the data-tuned controller and the measurement-tuned controller for week #1: Power consumption (Top). Number of working compressors (Bottom).

Table 7. Statistical errors from the controller comparison.

Quantity	Indices	Data-tuned controller		Measurement-tuned controller	
		With outliers	Without outliers	With outliers	Without outliers
Power (1h)	CVRMSE [%]	25.7	24	20.8	13.7
	NMBE [%]	2.9	4.2	-3.3	-0.2
Daily Energy	CVRMSE [%]	17.4	14.6	20.6	10.6
	NMBE [%]	4.4	5.9	-5.4	-0.4

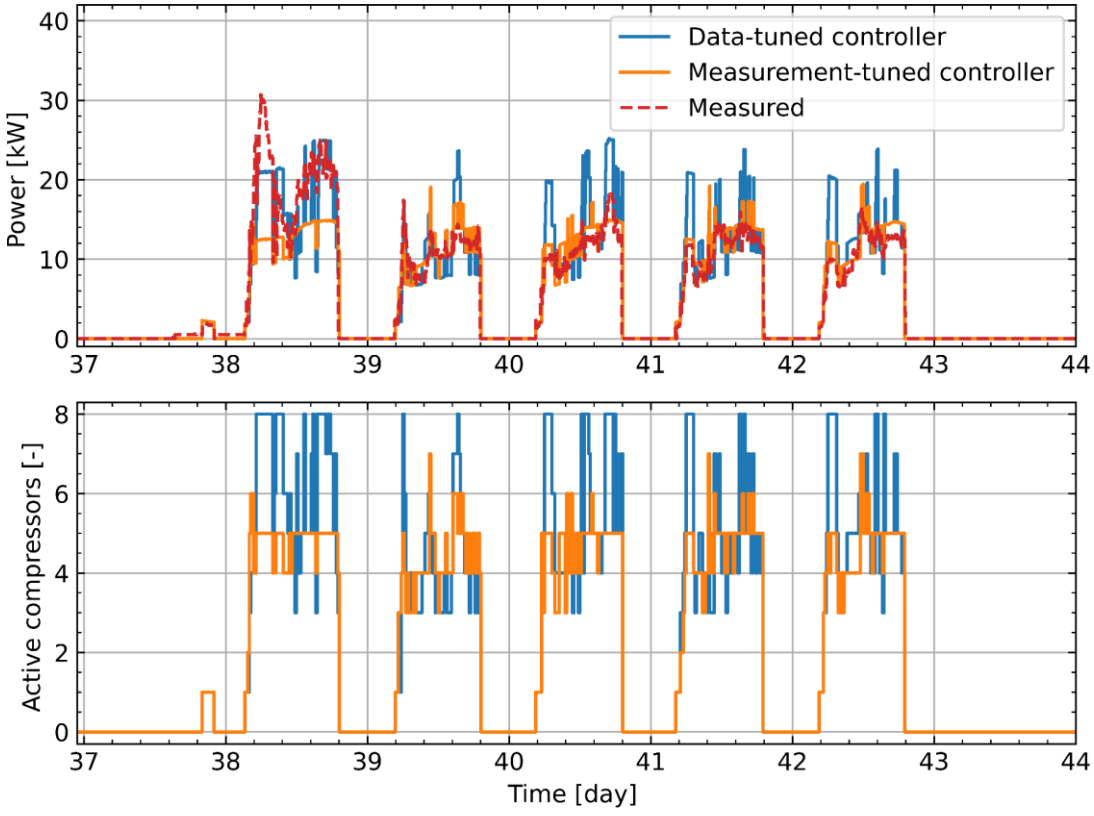

Figure 13. Comparison results between the data-tuned controller and the measurement-tuned controller for week #2: Power consumption (Top). Number of working compressors (Bottom).

Over the two-week period, the VRF daily energy consumption shows consistent results when comparing measured data and simulated data using both controllers.

Excluding the outliers, the CVRMSE and NMBE values for the data-tuned controller are 14.6% and 5.9%, respectively. In contrast, the measurement-tuned controller yields better performance with a CVRMSE of 10.6% and an NMBE of -0.4%. The same trend is observed when the results are extended to the entire cooling period.

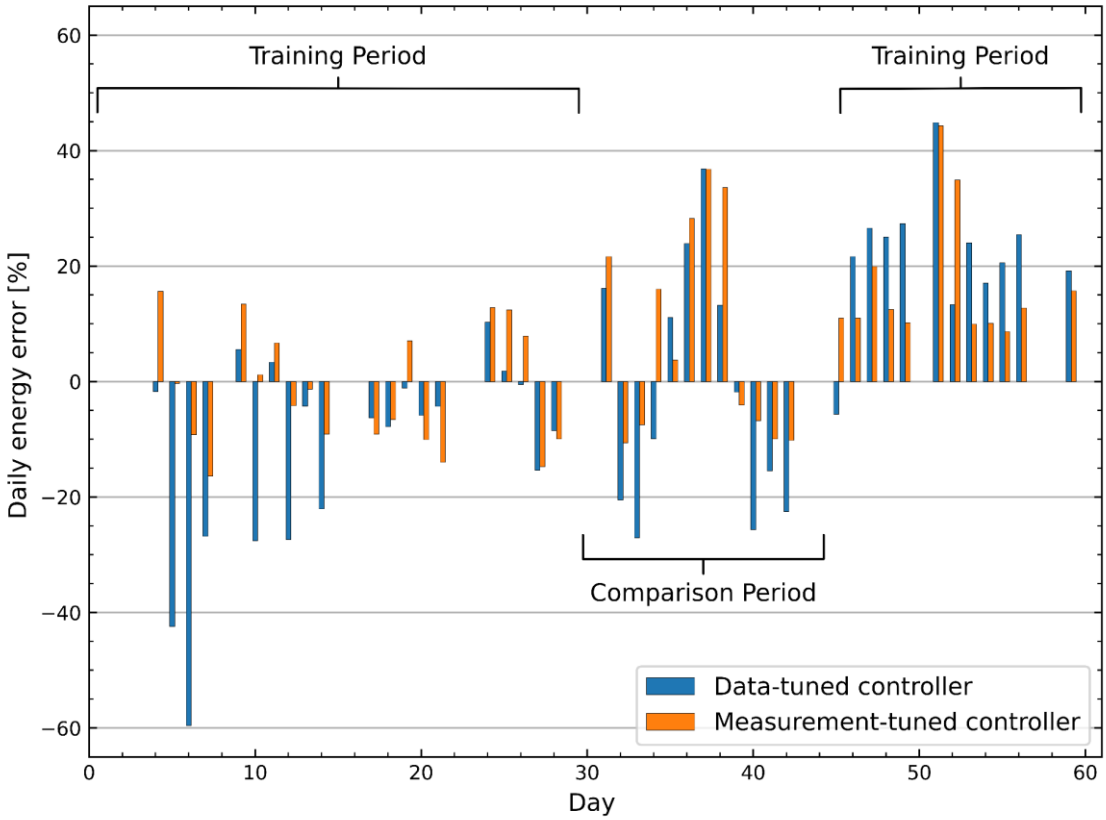

Figure 14. Daily energy relative error for both controllers during the training and comparison periods.

The performance of the two controllers is further evaluated by comparing their relative errors in the VRF simulated energy to the actual measurements, as illustrated in Figure 14. This evaluation considers both the training and comparison periods. As anticipated, the relative error with the measurement-tuned controller is generally lower during the training period, with a few exceptions. However, during the test period, although the measurement-tuned controller exhibits better overall prediction accuracy, as detailed in Table 7, there are instances where it results in a larger relative error.

The advantage of the measurement-tuned controller is further exemplified in Figure 15, where the disparity between the simulated and measured daily energy is noticeably reduced when this controller is employed. Additionally, this figure highlights that the outliers include days with the highest recorded VRF energy consumption, which accounts for their significant impact on the validation criteria (CVRMSE and NMBE).

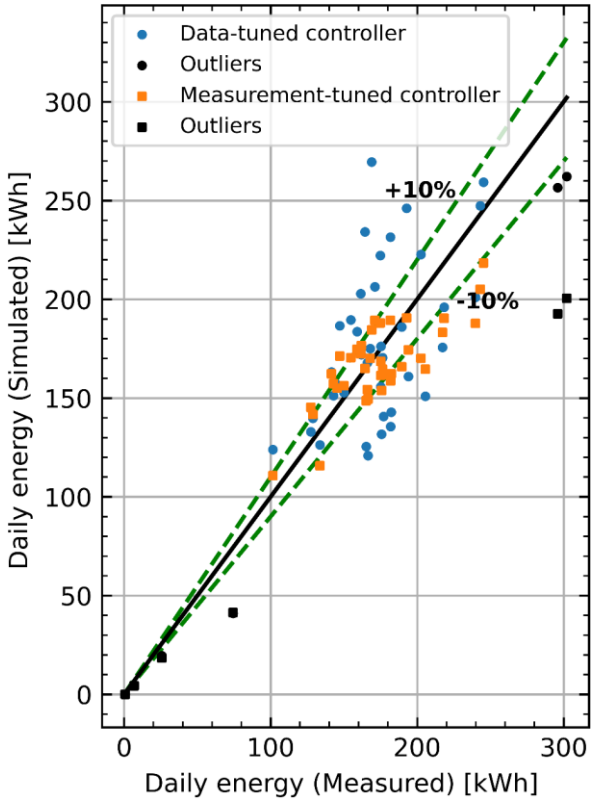

Figure 15. Comparison between the simulated and the measured daily energy.

6. Discussion

From the comparison results, it can be concluded that the VRF model is quite reliable in predicting the trend of compressors power variation and providing accurate assessments of total energy consumption during the cooling season within the limits set forth by ASHRAE guidelines. However, a closer examination of the comparison between the measured data and the simulation results reveals certain shortcomings in the model that

are worth noting:

(1) The model exhibits some spikes where it overestimates the system power consumption, which can be attributed to an inaccurate estimation of the number of working compressors by the capacity controller. This is primarily because the manufacturer data used to train the controller model does not include operation with low combination ratios. As a result, there is a bias towards operation with high combination ratios, which leads to an overestimation of the number of working compressors.

(2) The simplified vapor compression cycle used in the VRF model makes certain assumptions, including the assumption that there is no pressure drop in the refrigerant piping lines. However, to enhance the accuracy of the model, it is necessary to account for the effect of pressure drop. This is because pressure drops have a significant impact on the capacity of indoor and outdoor units, which in turn affects the required power at the compressor and the overall COP of the system. As P. Yan et al. (2012) noted, even a relatively modest increase in refrigerant piping length, from 2 meters to 20 meters, can result in a reduction in COP of 7.7% in a 2 IU VRF system.

Moreover, certain disparities between the measured and simulated results could be attributed to limitations in the collected data:

(1) The mixed air relative humidity is assumed to be constant at 50%, but it can vary throughout the day, particularly when IUs are first turned on. As lower air relative humidity results in decreased power consumption, uncertainties in humidity levels further contribute to explaining the differences between the simulated results and the measured data. For instance, when all 22 IUs are operational with outside and return air temperatures of 30°C (86°F) and 20°C

(68°F) respectively, the simulated power in the model varies by 13.4% when the relative humidity fluctuates from 0% to 100%.

(2) The return air temperature for the IUs is unknown and is estimated to be equal to the zone temperature. However, since fresh air temperature is typically lower than the zone temperature, this estimation tends to increase the VRF power consumption. For example, when all 22 IUs are operational with an outside air temperature of 30°C and a return air humidity of 50%, the simulated power in the model decreases by 7.7% when all return air temperatures decrease from 20°C to 15°C. Furthermore, as the return air temperature is unknown, an accurate evaluation of the actual cooling capacity of the zones is not feasible, as no other related parameter is measured. Thus, the collected data are not suitable for a proper model comparison based on the capacity.

(3) The measured data includes instances where the VRF system is not functioning in its normal manner. Since the model is not designed to account for these behaviors, these data points tend to increase the errors between the measured and simulated results.

Despite its inherent bias towards operation with high combination ratios, the model has demonstrated a noteworthy capacity to accurately predict the energy consumption of VRF systems. In scenarios where precise insight into the instantaneous behavior of VRF systems is essential, further enhancements can be achieved by incorporating onsite measurements. Beyond gathering all the necessary inputs for the model, it would be beneficial to collect these measurements over an extended period. This is particularly important since the model's controller relies on machine learning, which benefits from a comprehensive dataset for improved accuracy and robustness. Moreover, the decision tree algorithm was chosen due to its suitability for the problem

and its compatibility with implementation using Boolean logic. Despite efforts to fine-tune the model's hyperparameters, the predictive accuracy remains consistent within the same range. To enhance the compressor prediction accuracy, alternative machine learning methods such as ensemble learning could be adopted. This approach is effective in addressing the variation in performance exhibited by different machine learning models for the same problem. Ensemble learning involves training multiple machine learning models and combining their predictions to produce a refined outcome (Sagi & Rokach, 2018). In the realm of BEPS, ensemble learning models have been substantiated to outperform standalone machine learning models across various metrics (Konhäuser et al., 2022).

7. Conclusion

This study presented a new VRF heat pump model aimed towards multi-year simulations of VRF systems with multiple indoor units. The VRF model is based on a simplified vapor compression cycle and includes the following features: (1) component models for both indoor units (IU) and outdoor units (OU), providing modularity to accommodate various VRF configurations, (2) multiple compressors operation to facilitate dynamic capacity adjustments, (3) a capacity control strategy that enables the selection of the optimal number of working compressors based on the operational conditions, particularly during part-load operation. Additionally, a calibration procedure is proposed to evaluate the model's parameters. The control strategy and parameter estimation procedure are developed by leveraging manufacturer data, ensuring comprehensive representation of commercial VRF systems without necessitating knowledge of their operational specifics.

IU and OU models were implemented in Modelica, and the calibration procedure was implemented in Python. The model is validated in cooling mode using data recorded from the VRF system that serves the first floor of the former ASHRAE Headquarters Building in Atlanta, comprised of 22 indoor units, 2 outdoor units and 8 compressors. Results showed that the model accurately predicted the total energy consumption during a two-month cooling period with a relative error, an NMBE, and a CVRMSE of 1%, 1.6%, and 16.7%, respectively, when compared to monitored data. The accuracy of the model could be further improved by incorporating measured data into the training of the capacity controller model.

The developed VRF model provides a solid foundation for the development of a new VRF Heat Recovery (VRF-HR) model. The development of the VRF-HR model is an important step towards achieving a more comprehensive simulation of the VRF system's performance. This enhanced model will enable the simulation of simultaneous heating and cooling operation, thereby providing a more comprehensive and realistic depiction of the VRF system's performance. To validate the VRF-HR model, it will be tested against the complete data recorded from the ASHRAE Headquarters Building. Future efforts will also be focused on improving the model's accuracy, particularly with regards to the pressure drop evaluation and the capacity control strategy.

Acknowledgment

The authors acknowledge the support of the Natural Sciences and Engineering Research Council of Canada (NSERC), [funding reference number RGPIN-2018-04471]. The authors also acknowledge the support of the NSERC, the Trottier Energy Institute and Hydro-Québec for scholarships awarded to the first author. This study leveraged measured data kindly provided by Dr. Jeffrey Spitler and Laura Southard, for which the authors are deeply appreciative.

References

ASHRAE. (2014). Measurement of Energy and Demand Savings *ASHRAE Guideline 14*.

Braun, J. E., Klein, S. A., & Mitchell, J. W. (1989). Effictiveness models for cooling towers and cooling coils. *ASHRAE Transactions, 95*(2), 164-174.

Chen, Y., Halm, N., Groll, E. A., & Braun, J. E. (2000). *A Comprehensive Model of Scroll Compressors, Part II: Overall Scroll Compressor Modeling.* Paper presented at the International Compressor Engineering Conference at Purdue Purdue University, West Lafayette, IN.

Cheung, H., & Braun, J. E. (2014). Component-based, gray-box modeling of ductless multi-split heat pump systems. *International Journal of Refrigeration, 38*, 30-45. doi:10.1016/j.ijrefrig.2013.10.007

Coakley, D., Raftery, P., & Keane, M. (2014). A review of methods to match building energy simulation models to measured data. *Renewable and Sustainable Energy Reviews, 37*, 123-141. doi:10.1016/j.rser.2014.05.007

Elliott, M. S., & Rasmussen, B. P. (2009). A model-based predictive supervisory controller for multi-evaporator HVAC systems. 3669-3674. doi:10.1109/acc.2009.5160498

Goetzler, W. (2007). Variable refrigerant flow systems. *Ashrae Journal*.

Hong, T., Sun, K., Zhang, R., Hinokuma, R., Kasahara, S., & Yura, Y. (2016). Development and validation of a new variable refrigerant flow system model in EnergyPlus. *Energy and Buildings, 117*, 399-411. doi:10.1016/j.enbuild.2015.09.023

Hydeman, M., & Gillespie, K. (2002). Tools and Techniques to Calibrate Electric Chiller Component Model. *ASHRAE Transactions, 108*(1), 733–741.

Jin, H., & Spitler, J. D. (2002). A parameter estimation based model of water-to-water heat pumps for use in energy calculation programs. *ASHRAE Transactions, 108*(Part 1).

Kibo, K., Masafumi Hirota, Yuta Teranishi, Yoichi Miyaoka, Katsuaki Nagamatsu, Takashi Namiwo, Yoshinori Yura, Takuya Kotani and Shinichi Kasahara. (2016). *Development of high efficiency VRF systems under partial heat load for commercial buildings*.

Kim, D., Cox, S. J., Cho, H., & Im, P. (2018). Model calibration of a variable refrigerant flow system with a dedicated outdoor air system: A case study. *Energy and Buildings, 158*, 884-896. doi:10.1016/j.enbuild.2017.10.049

Konhäuser, K., Wenninger, S., Werner, T., & Wiethe, C. (2022). Leveraging advanced ensemble models to increase building energy performance prediction accuracy in the residential building sector. *Energy and Buildings, 269*, 112242. doi:10.1016/j.enbuild.2022.112242

Li, P., Li, Y., Seem, J. E., Qiao, H., Li, X., & Winkler, J. (2014). Recent advances in dynamic modeling of HVAC equipment. Part 2: Modelica-based modeling. *HVAC&R Research, 20*(1), 150-161. doi:10.1080/10789669.2013.836876

Li, Y., Wu, J., & Shiochi, S. (2009). Modeling and energy simulation of the variable refrigerant flow air conditioning system with water-cooled condenser under cooling conditions. *Energy and Buildings, 41*(9), 949-957. doi:10.1016/j.enbuild.2009.04.002

Lin, X., Lee, H., Hwang, Y., & Radermacher, R. (2015). A review of recent development in variable refrigerant flow systems. *Science and Technology for the Built Environment, 21*(7), 917-933. doi:10.1080/23744731.2015.1071987

Mbaye, A., & Cimmino, M. (2021). *A parameter-estimation model for variable refrigerant flow heat pump systems*. Paper presented at the 13th IEA Heat Pump Conference, Jeju Korea.

McElgin, J., & Wiley, D. C. (1940). Calculation of coil surface areas for air cooling and dehumidification. *Heating, Piping and Air Conditioning, 12*(1), 195-201.

Pachano, J. E., Peppas, A., & Bandera, C. F. (2022). Seasonal adaptation of VRF HVAC model calibration process to a mediterranean climate. *Energy and Buildings, 261*, 111941. doi:10.1016/j.enbuild.2022.111941

Pedregosa, F., Varoquaux, G., Gramfort, A., Michel, V., Thirion, B., Grisel, O., . . . Duchesnay, E. (2011). Scikit-learn: Machine Learning in Python. *Journal of Machine Learning Research, 12*, 2825-2830. doi:
https://doi.org/10.48550/arXiv.1201.0490

Petrus, I. (2021). The Proprietary Roadblocks Stunting the Future of VRF Design. *Engineered Systems*.

Raustad, R. (2013). A Variable Refrigerant Flow Heat Pump Computer Model in EnergyPlus. *Ashrae Transactions 2013, Vol 119, Pt 1, 119*, 299-308.

Reddy, T. A. (2006). Literature review on calibration of building energy simulation programs: Uses, problems, procedures, uncertainty, and tools. *Ashrae Transactions 2006, Vol 112, Pt 1, 112*, 226-240.

Robertson, J., Polly, B., & Collis, J. (2013). *Evaluation of Automated Model CalibrationTechniques for Residential Building Energy Simulation*. Retrieved from

Sagi, O., & Rokach, L. (2018). Ensemble learning: A survey. *WIREs Data Mining and Knowledge Discovery, 8*(4). doi:10.1002/widm.1249

Sharma, C., & Raustad, R. (2013). Compare Energy Use in Variable Refrigerant Flow Heat Pumps Field Demonstration and Computer Model. *Ashrae Journal*.

Southard, L. E., Liu, X., & Spitler, J. D. (2014a). Performance of HVAC Systems at ASHRAE HQ Part.1. *Ashrae Journal, 56*(9), 14-22.

Southard, L. E., Liu, X., & Spitler, J. D. (2014b). Performance of HVAC Systems at ASHRAE HQ Part.2. *Ashrae Journal, 56*(12), 12-23.

Sun, H., Ding, G., Hu, H., Ren, T., Xia, G., & Wu, G. (2017). A general simulation model for variable refrigerant flow multi-split air conditioning system based on graph theory. *International Journal of Refrigeration, 82*, 22-35. doi:10.1016/j.ijrefrig.2017.07.003

Tu, Q., Zou, D., Deng, C., Zhang, J., Hou, L., Yang, M., . . . Feng, Y. (2016). Investigation on output capacity control strategy of variable refrigerant flow air conditioning system with multi-compressor. *Applied Thermal Engineering, 99*, 280-290. doi:10.1016/j.applthermaleng.2015.12.102

Virtanen, P., Gommers, R., Oliphant, T. E., Haberland, M., Reddy, T., Cournapeau, D., . . . SciPy, C. (2020). SciPy 1.0: fundamental algorithms for scientific computing in Python. *Nat Methods, 17*(3), 261-272. doi:10.1038/s41592-019-0686-2

Wetter, M., Fuchs, M., Grozman, P., Helsen, L., Jorissen, F., Müller, D., . . . Thorade, M. (2015). *IEA EBC Annex 60 Modelica Library - An international collaboration to develop a free open-source model library for buildings and community energy systems*. Paper presented at the International Conference of the International Buildings Performance Simulation Association, Hyderabad.

Winandy, E., Saavedra, C., & Lebrun, J. (2002). Experimental analysis and simplified modelling of a hermetic scroll refrigeration compressor. *Applied Thermal Engineering, 22*(2), 107-120. doi:10.1016/s1359-4311(01)00083-7

Wu, C., Xingxi, Z., & Shiming, D. (2005). Development of control method and dynamic model for multi-evaporator air conditioners (MEAC). *Energy Conversion and Management, 46*(3), 451-465. doi:10.1016/j.enconman.2004.03.004

Xiangguo, X., Yan, P., Shiming, D., Liang, X., & Mingyin, C. (2013). Experimental study of a novel capacity control algorithm for a multi-evaporator air conditioning system. *Applied Thermal Engineering, 50*(1), 975-984. doi:10.1016/j.applthermaleng.2012.08.007

Yan, H., Deng, S., & Chan, M.-y. (2016). A novel capacity controller for a three-evaporator air conditioning (TEAC) system for improved indoor humidity control. *Applied Thermal Engineering, 98*, 1251-1262. doi:10.1016/j.applthermaleng.2016.01.052

Yan, P., Xiangguo, X., Liang, X., & Shiming, D. (2012). A modeling study on the effects of refrigerant pipeline length on the operational performance of a dual-evaporator air conditioning system. *Applied Thermal Engineering, 39*, 15-25. doi:10.1016/j.applthermaleng.2012.01.006

Yun, G. Y., & Song, K. (2017). Development of an automatic calibration method of a VRF energy model for the design of energy efficient buildings. *Energy and Buildings, 135*, 156-165. doi:10.1016/j.enbuild.2016.11.060

Zhou, Y. P., Wu, J. Y., Wang, R. Z., & Shiochi, S. (2007). Energy simulation in the variable refrigerant flow air-conditioning system under cooling conditions. *Energy and Buildings, 39*(2), 212-220. doi:10.1016/j.enbuild.2006.06.005

Zhou, Y. P., Wu, J. Y., Wang, R. Z., Shiochi, S., & Li, Y. M. (2008). Simulation and experimental validation of the variable-refrigerant-volume (VRV) air-conditioning system in EnergyPlus. *Energy and Buildings, 40*(6), 1041-1047. doi:10.1016/j.enbuild.2007.04.025

Zhu, Y., Jin, X., Du, Z., Fan, B., & Fu, S. (2013). Generic simulation model of multi-evaporator variable refrigerant flow air conditioning system for control analysis. *International Journal of Refrigeration, 36*(6), 1602-1615. doi:10.1016/j.ijrefrig.2013.04.019

Zhu, Y., Jin, X., Du, Z., & Fang, X. (2015). Online optimal control of variable refrigerant flow and variable air volume combined air conditioning system for energy saving. *Applied Thermal Engineering, 80*, 87-96. doi:10.1016/j.applthermaleng.2015.01.030